PCCP

RSC Publishing

PAPER

View Article Online
View Journal | View Issue

Cite this: *Phys. Chem. Chem. Phys.*, 2013, **15**, 7777

Neutron reflectometry studies on the lithiation of amorphous silicon electrodes in lithium-ion batteries

B. Jerliu,[a] L. Dörrer,[a] E. Hüger,[a] G. Borchardt,[a] R. Steitz,[b] U. Geckle,[c] V. Oberst,[c] M. Bruns,[c] O. Schneider[d] and H. Schmidt*[a]

Received 10th December 2012,
Accepted 2nd April 2013

DOI: 10.1039/c3cp44438d

www.rsc.org/pccp

Neutron reflectometry is used to study *in situ* the intercalation of lithium into amorphous silicon electrodes. The experiments are done using a closed three-electrode electrochemical cell setup. As a working electrode, an about 40 nm thick amorphous silicon layer is used that is deposited on a 1 cm thick quartz substrate coated with palladium as a current collector. The counter electrode and the reference electrode are made of lithium metal. Propylene carbonate with 1 M $LiClO_4$ is used as an electrolyte. The utility of the cell is demonstrated during neutron reflectometry measurements where Li is intercalated at a constant current of 100 μA (7.8 μA cm^{-2}) for different time steps. The results show (a) that the change in Li content in amorphous silicon and the corresponding volume expansion can be monitored, (b) that the formation of the solid electrolyte interphase becomes visible and (c) that an irreversible capacity loss is present.

1. Introduction

Lithium-ion batteries are widely developed and used as rechargeable power sources for portable electronic devices and will be essential in the field of automotive transportation.[1–3] For the latter applications improvements in energy density and thus driving range/battery weight, power density, cycle life and costs are required.[4] Processes at the electrodes during charging and discharging cycles play a key role in understanding and optimizing these batteries. In general, the electrode reactions are based on intercalation–de-intercalation of Li into solid hosts or on solid state reactions including formation of Li compounds.[5] These solid state processes often are rather slow and therefore lead to a low charge–discharge rate and to low power densities. Consequently, there is a strong need for a quantitative understanding of electrode processes in promising electrode candidate materials showing a high energy density. This requires the investigation of both, processes at electrolyte/electrode interfaces and processes within the solid host materials, including determination of intercalation kinetics and of intercalation pathways. In order to accomplish this task, electrochemical methods must be combined with other methods for characterization of material properties.

In the literature, there exist numerous *ex situ* characterizations of the electrode after electrochemical cycling in order to gain insight into the problem discussed above.[6–11] However, such experiments have the drawback that not the actual state of the intercalation process is monitored and consequently they are of limited significance. Consequently, there is a strong need for studies of the intercalation process during the operation of the electrochemical cell (*in operando* or *in situ* studies).[12] Such studies were already performed using transmission electron microscopy,[13–14] electrochemical strain microscopy,[15] nuclear magnetic resonance,[16] and X-ray scattering[17–19] on different types of electrode materials. In the present paper, *in operando* neutron reflectometry measurements on the intercalation of lithium at electrodes during charging and discharging are presented. For the realization of such experiments a well-sealed electrochemical cell was constructed that allows working in ambient air at neutron facilities.

In the context of electrochemistry, neutron reflectometry (NR) measurements so far have been mainly applied for the study of redoxactive inorganic[20] and organic films[21] and conducting polymers.[22] Further studies include the structure and transformations in monolayer adsorbate films,[23] polyelectrolytes,[24] electrodeposited metal bilayers[25] and corrosion of metal films.[26] There is only a several year old study, concerned with lithium-ion batteries,[27]

[a] *Technische Universität Clausthal, Institut für Metallurgie, Abteilung Thermochemie und Mikrokinetik, Robert-Koch-Str. 42, 38678 Clausthal-Zellerfeld, Germany. E-mail: harald.schmidt@tu-clausthal.de*
[b] *Helmholtz-Zentrum Berlin für Materialien und Energie GmbH, Hahn-Meitner-Platz 1, 14109 Berlin, Germany*
[c] *Karlsruhe Institute of Technology, Institute for Applied Materials (IAM-ESS), Eggenstein-Leopoldshafen, Germany*
[d] *Technische Universität München, Physics Department, James-Franck-Str. 1, 85748 Garching, Germany*

where the intercalation of Li into anatase (TiO_2) is investigated, demonstrating the possibility of realizing such experiments. Recently, NR was also used to study solid electrolyte interphase (SEI) formation at copper surfaces.[28] In addition, there are publications on Li intercalation based on neutron diffractometry,[29] small angle neutron scattering,[30] and neutron depth profiling[6,31] as well as a neutron radiography study[32] to investigate bubble formation at electrodes.

In the present study, we carried out experiments on the lithiation of amorphous silicon, which is a promising negative electrode material for Li-ion batteries due to its high theoretical specific capacity of about 4000 mA h g^{-1} (ref. 3), corresponding to the reaction

$$Si + xLi^+ + xe^- \rightarrow Li_xSi \quad (x \leq 4)$$

Despite numerous studies on intercalation, the oxidation–reduction process, and cycling stability[33–38] based on electrochemical methods, little is known about the mode and kinetics of intercalation of lithium inside amorphous silicon electrodes. Is charging taking place by a diffusion-controlled movement of a phase boundary (*e.g.* Li_xSi) parallel to the electrode surface or by diffusion or interface controlled solid solution formation? Studies on morphological and phase changes during charging, given in the literature, show that over a wide range of cell potentials the electrode remains essentially amorphous.[39,40] At low potentials ($x \sim 4$ for Li_xSi) a reversible crystallization to a metastable crystalline $Li_{15}Si_4$ phase is observed,[39,41] however, for relatively thick electrode films only.

In the present paper we describe the design of a closed three-electrode electrochemical cell for NR studies of the electrochemical Li intercalation in a thin film amorphous silicon electrode. The utility of the cell is demonstrated by NR measurements during an intercalation cycle at a constant current of 100 μA (7.8 μA cm^{-2}). The relative sensitivity of neutrons on lithium (in comparison to X-rays) and the ability of neutrons to pass through relatively thick solid substrates allow us to probe lithium density profiles perpendicular to the surface of reflection. Simulations of the reflectivity profiles using appropriate software, *e.g.* Parratt32,[42] allow us to derive the scattering length density profile and the Li concentration inside the electrode. This gives direct insight into the Li concentration and volume changes taking place during intercalation.

2. Experimental details

The design of the electrochemical cell is shown in Fig. 1 and an image of the cell is displayed in Fig. 2. A thin film arrangement is used to produce a large area working electrode necessary for NR experiments. The cell is constructed with three electrodes. The working electrode is made of a quartz block as a substrate, which is coated with a thin palladium layer as a back contact and a current collector. The electrode material of amorphous silicon (about 40 nm) is deposited on top of the palladium. Here, a circular design with an electrode diameter of 40.5 mm (contact area to electrolyte) is used. As the counter electrode

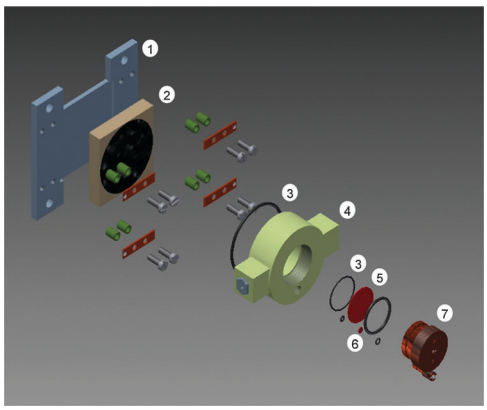

Fig. 1 Schematic sketch of the electrochemical cell: (1) 5 mm thick aluminium ground plate; (2) 10 mm thick Pd coated quartz substrate with an amorphous silicon electrode on it (circle); (3) Kalrez® gaskets; (4) 20 mm thick high density polyethylene base; (5) Li counter electrode; (6) Li reference electrode; and (7) copper base.

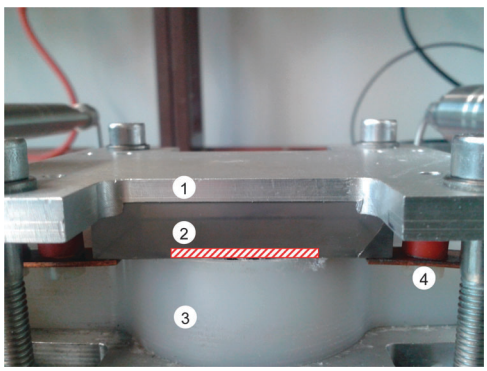

Fig. 2 Image of the cell: (1) aluminium ground plate; (2) quartz substrate and electrode; (3) polyethylene housing; and (4) contacts to potentiostat. The shaded area depicts the position and the cross section of the neutron beam which is incident perpendicular to the paper plane (not to scale).

and the reference electrode metallic lithium (1.5 mm foil, 99.9%, Alfa Aesar) is used. The working and counter electrodes are separated by Kalrez® gaskets forming a cell with a total volume of 1.4 ml. Additionally, a separator with a thickness of 20 μm (Brückner Maschinenbau, Germany) is introduced between the two electrodes. The lithium electrodes are sealed against high density polyethylene housing also using Kalrez® gaskets. The cell is filled with the electrolyte through two ports bored into the polyethylene. As an electrolyte, propylene carbonate (Sigma Aldrich, anhydrous, 99.7%) with 1 M $LiClO_4$ (Sigma Aldrich, lithium perchlorate, battery grade, dry, 99.99% trace metal basis) is used. Before the lithium salt was dissolved in the non-aqueous solvent the latter was dried for one week under argon using molecular sieves (Carl Roth, 3 Å). The electrochemical cell was assembled within an argon filled glove box (water content < 0.1 ppm, oxygen content < 0.1 ppm).

The working electrode was prepared in the following way: first an approximately 80 nm thick palladium layer was deposited on the polished quartz block by RF magnetron sputtering. Deposition was done at a rate of 11 nm min^{-1}, using argon (6.0)

sputter gas at an operating pressure of 0.3 Pa, and a sputtering power of 150 W at room temperature. Afterwards a 40 nm thick amorphous silicon layer was sputtered using a RF power of 75 W. The deposition rate was 8 nm min^{-1} at an operating pressure of 0.2 Pa. The sputter set-up in detail is described elsewhere.[43]

Grazing incidence X-ray diffraction (Bruker D5000, Co $K\alpha_1$, 40 kV) showed characteristic sharp Bragg peaks of palladium and a several degree broad reflection corresponding to amorphous silicon. This confirms the amorphous nature of the electrode material. Additional crystallographic phases were not detected.

The neutron measurements were done using the classical $\theta/2\theta$ mode of operation and a monochromatic beam at a wavelength of 0.466 nm at the V6 reflectometer located at the Helmholtz-Zentrum, Berlin, Germany. Data were recorded in the range between 0.06° and 1.7° incident angles in the vertical scattering plane of the instrument during a total time of about 5 h per run. Here, the quartz substrate is the incoming medium for neutrons. During a NR experiment the collimated neutron beam (40 mm horizontal slits, 0.5 mm vertical slits) is directed through the side of the quartz block (see Fig. 2). The neutrons are reflected from the SiO_2/Pd/Si/electrolyte interfaces, exit the quartz on the opposite side and are detected afterwards. ^{3}He pencil detectors, offset from each other by 0.44° in 2θ, are used for recording the scattered intensity in the specular and background channel, respectively. The information obtained from NR is the reflected intensity perpendicular to the reflecting interface. The reflectivity data were corrected for footprint and background. Data analysis was performed on basis of Parratt's recursion algorithm using the Parratt32 software package.[42]

Electrochemical intercalation was carried out using a computer controlled potentiostat (BioLogic, model SP-150). Lithium was galvanostatically inserted and extracted at a current of 20 or 100 μA, respectively, resulting in intercalation potentials between 2.9 and 0.2 V *vs.* Li.

3. Results and discussion

The experiments were conducted on an assembled cell, filled completely with the electrolyte that was mounted on the goniometer stage of the reflectometer. First a neutron reflection scan was made without applying any current and before any intercalation was initiated. This state is termed the *virgin state*. The results are shown in Fig. 3(a) as open circles. Since the neutron beam hits the interface coming from a denser medium (SiO_2), an edge of total reflection is not observed. We see that a complex reflectivity pattern is found with numerous fringes, which result from the interference of neutrons reflected at the SiO_2/Pd/Si/electrolyte interfaces. The fit results with Parratt32, based on a box-model, are also shown in Fig. 3(a) as lines. The resulting parameters are given in Table 1 and the corresponding scattering length density (SLD) is shown in Fig. 4(a). From the determined SLD, mass densities of the compounds are calculated using the NIST online resource database[44] (see also Table 1). The mass densities found correspond very well to literature values of bulk samples for quartz, palladium and amorphous silicon. The slightly higher value for propylene

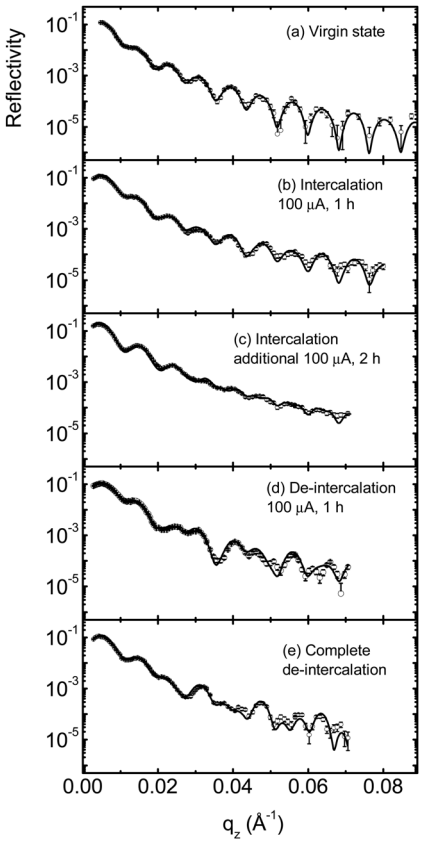

Fig. 3 Neutron reflectometry patterns measured at different stages during an intercalation cycle (open circles). Also shown are the fitting results using Parratt32 (lines), which correspond to the SLDs of Fig. 4.

carbonate is attributed to the small amount of $LiClO_4$ dissolved in the electrolyte, which was neglected in the calculation. A closer inspection of results revealed that an appropriate fitting of the reflectivity could be obtained only if a thin (6 Å) additional layer with a low SLD of 1.3×10^{-6} Å^{-2} is incorporated between the quartz substrate and the palladium. Otherwise the strong fringes at high scattering vectors cannot be reproduced. We associate this ''intermediate layer'' to a low density layer that results from lattice mismatch by sputtering polycrystalline palladium on the single crystalline quartz substrate. The existence of an additional surface layer (*e.g.* an oxide) with a thickness of more than 3–5 Å and with a different SLD between amorphous silicon and the electrolyte is not indicated by the present measurements. The interface roughness between palladium and silicon was determined by fitting to be (1.4 ± 0.3) nm. In contrast, the situation for the roughness of the Si/electrolyte interface is more difficult. A fixed input value of this roughness in the range between 0 and 4 nm in Parratt32 fitting results in identical reflectivities within error limits. Consequently, this roughness cannot be determined exactly by fitting. For further analysis, we also measured separately the surface roughness of palladium and silicon films directly sputtered on quartz by atomic force microscopy (AFM). For palladium we found a roughness (RMS) value of 1.1 nm in good accordance with the roughness of the Pd/Si interface obtained

Table 1 Parameters of the Parratt32 fits of the electrode system in the virgin state. Errors correspond to a 10% increase of χ^2 of the best fit with respect to the fitted parameter only. Quantities (roughness) with no errors were kept fixed during the fit in order to omit unreliable fitting results. Also given are mass densities calculated from SLDs,[44] and mass densities from the literature

Layers of the box-model	Thickness (Å)	SLD ($\times 10^{-6}$ Å^{-2})	Roughness (Å)	Mass density (g cm^{-3})	Mass density from the literature (g cm^{-3})
Quartz (SiO_2)	n/a	4.15 ± 0.06	n/a	2.63 ± 0.04	2.65 (ref. 50)
Intermediate layer	6 ± 2	1.3 ± 0.9	0	n/a	n/a
Palladium	760 ± 9	3.95 ± 0.05	0	11.80 ± 0.15	12.02 (ref. 48)
Amorphous silicon	425 ± 25	1.95 ± 0.05	14 ± 3	2.19 ± 0.05	2.19–2.29 (ref. 7)
Propylene carbonate ($C_4H_6O_3$)	n/a	1.85 ± 0.13	13	1.45 ± 0.10	1.21 (ref. 49)

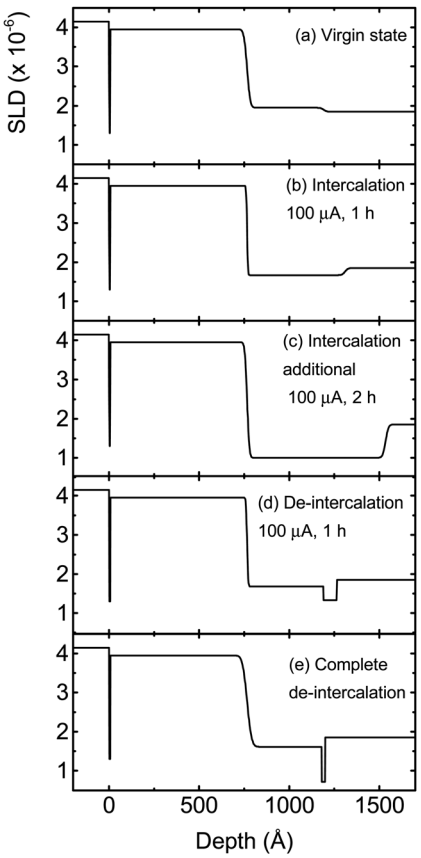

Fig. 4 SLD profiles corresponding to the fits of the NR data in Fig. 3.

using Parratt32. Further, AFM gives a roughness of 1.3 nm for the Si sample. Due to the problem mentioned above, this is now used as a fixed input value for the Parrat32 calculations (see Table 1). As a result, the electrode in its virgin state can be described very well by the neutron reflectivity data.

During lithiation, Li from the electrolyte is transferred over the interface and reductively incorporated into the amorphous silicon electrode. During this process the formation of amorphous Li_xSi (x = 0–4.2) is indicated.[39] In the present work, a stepwise lithiation procedure was applied with several galvanostatic charging steps at a defined current, I, for a defined time period, t, followed by discharging steps (see Fig. 5(a)). After each step, current was interrupted and the system was allowed to relax until equilibrium was established, as indicated by a constant potential. Afterwards, a neutron reflectivity pattern was recorded and the results were fitted using Parratt32. Thereafter, the next galvanostatic step was done. Characteristic potential *vs.* time curves for intercalation–de-intercalation at currents of 100 μA are shown in Fig. 5(b). Current application first leads to a rapid departure of the electrode potential from the open circuit value of 2.9 V *vs.* Li, and thereafter to a more gradual shift in electrode potential towards lower values with progressive intercalation (see Fig. 5(b)).

In the first step, a current of I = 20 μA (1.6 μA cm^{-2}) has been applied for a time of t = 1 h (not shown in Fig. 5(b)), leading apparently to a theoretical specific capacity, C, of 0.17 A h g^{-1} and to a relative Li fraction in Li_xSi of x = 0.17 using the equations

$$C = \frac{It}{m_{Si}} \quad (1)$$

and

$$x = \frac{ItM_{Si}}{Fm_{Si}} \quad (2)$$

where $m_{Si} \approx 1.2 \times 10^{-4}$ g is the actual silicon electrode mass, F = 96 487 C mol^{-1} is the Faraday constant, and M_{Si} = 28.09 g mol^{-1} is the molar mass of silicon. The quantities are calculated for a radius of the circular silicon electrode of 20.25 mm (contact area), a layer thickness of 42.5 nm and a mass density of 2.19 g cm^{-3}.

During this galvanostatic charging step, the potential between the working electrode and the reference electrode decreased from about 2.92 to 0.75 V. However, after this charging step, during the equilibration period, the potential increased again to its initial value. The corresponding neutron reflectivity pattern after the equilibration period was completely identical to that of the virgin state. This means that no significant amount of Li was introduced into the electrode during this step. The strong potential changes were caused by charge transfer effects at the electrode/electrolyte interface, and possibly by a change in the cell resistance. The absence of Li insertion in this experiment is consistent with voltammetric studies carried out subsequently to the work described in this paper, using the same cell, where characteristic peaks of Li insertion and de-insertion were below 0.6 V. It also agrees with reports from the literature, where Li insertion at potentials above 0.4–0.6 V was not observed, and where also reduced Li insertion was found in the first (voltammetric) cycle.[8,45,46] These findings were in part explained with electrolyte decomposition

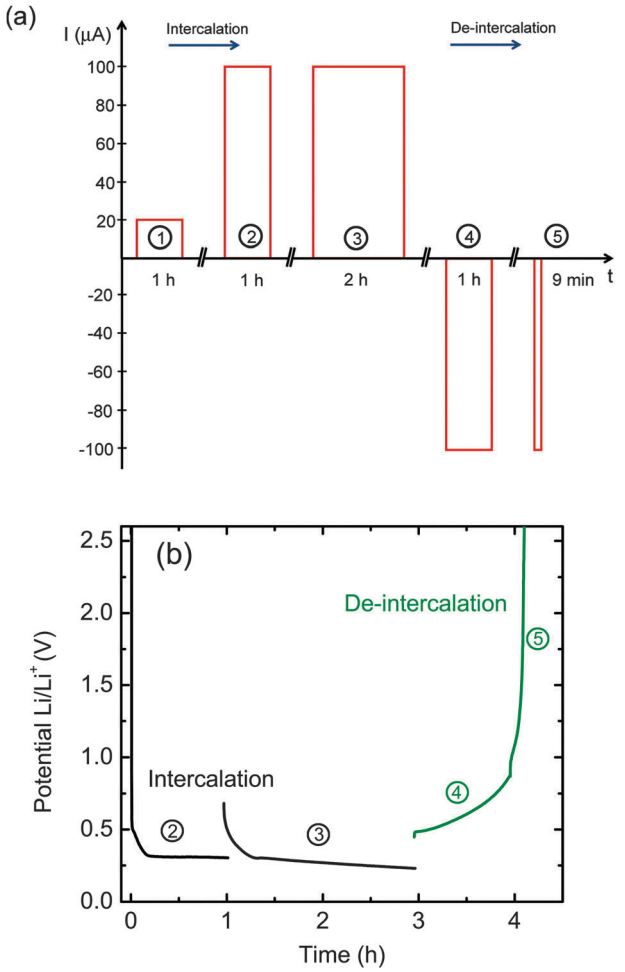

Fig. 5 (a) Flow chart of the current applied to the electrode for the different intercalation steps. During the interruption of intercalation as indicated at the abscissa, the system was allowed to relax for about 1 h and afterwards the neutron reflectometry measurements were done, which last about 5 h. (b) Galvanostatic charge–discharge curves cycled at a constant current of 100 μA for various time steps. The numbers correspond to the intercalation steps given in Tables 2 and 3.

and the formation of a solid electrolyte interface (SEI). For such a layer no evidence was seen in the NR data recorded after this first step.

In a second step, a higher current of 100 μA (7.8 μA cm^{-2}) was applied for 1 h. The corresponding potential decreased to 0.3 V (see Fig. 5(b)), but increased during equilibration to a value of only 0.68 V indicating that Li intercalation took place. This is also reflected in the neutron reflectivity pattern of Fig. 3(b). Clear changes occur in comparison to the virgin state. This shows that intercalation effectively starts at potentials below 0.75 V and is characterised by the flat part of the curve in Fig. 5(b) for times larger than 0.14 h (at 100 μA). Using eqn (1) and (2) one obtains $C = 0.83$ A h g^{-1} and $x = 0.87$ for that second intercalation step.

Finally, charging was completed by an additional step of 100 μA for 2 h. The maximum amount of charge introduced corresponded to a total capacity of 2.50 A h g^{-1} and $x = 2.61$. In order to avoid the destruction of the electrode by stress effects in these first experiments, intercalation was ended at this point and de-intercalation was started after the NR measurement. The direction of the current was reversed and two de-intercalation steps followed, the first one at 100 μA for 1 h and the second one at 100 μA for additional 9 min, which led to complete de-intercalation as seen by the rapid increase towards the potential of pure silicon in Fig. 5(b). As obvious from Fig. 3 the neutron reflectivity profiles change after each step, indicating that the intercalation process can be effectively monitored by NR. An interesting point is that after complete de-intercalation the virgin pattern is not restored (Fig. 3(a)and (e)). Slight but detectable differences are still visible. This confirms that charging–discharging is an irreversible process and a non-negligible amount of charge remains present in the electrode. This is also indicated by the fact that intercalation and de-intercalation times are not identical, which is known from the literature on electrochemical experiments,[47] and which is also demonstrated here by the NR experiments in a direct way. In the literature, this irreversible charge is attributed to the formation of a SEI during intercalation.[47] As known from the literature, lithiation and de-lithiation pathways can be distinctively different.[29]

For further analysis, all reflectivity curves of Fig. 3 are fitted by a box-model using Parratt32 and the corresponding SLD curves are given in Fig. 4. The resulting fit parameters of all experiments are given in Table 2. The fit parameters of the quartz block, of the electrolyte and of the intermediate layer as given in Table 1 for the virgin state are kept constant in the fitting procedure of the intercalated samples. As demonstrated in the literature,[51] only very small amounts of Li (about 1 at%) are incorporated into palladium by electrochemical lithiation using the same liquid electrolyte as in the present experiments. Consequently, the influence on our experiments is expected to be marginally small and the SLD of the Pd layer is assumed to be also unchanged during intercalation. The only parameters that are significantly modified during charging in comparison to the virgin state are the thickness and the SLD of the amorphous silicon–lithium layer (see Table 2). The interface roughness of all layers varies in the ±5 Å range in a non-systematic way, which means that this variation is not correlated to the lithiation process. As can be seen from Table 2, the thickness of the amorphous silicon layer increases, while at the same time the SLD decreases significantly. This can be interpreted as the increasing incorporation of Li into the silicon matrix. Due to the equilibration period after each intercalation step, it is assumed that Li is homogeneously distributed within the silicon electrode and that the Li concentration and SLD are constant within the Si layer. The Li incorporation is accompanied by a tremendous volume expansion, reflected in the thickness change of the Si layer (Table 2). Consequently, the change in SLD during lithiation is triggered by two factors: (1) the volume expansion and (2) the additional amount of Li inside the silicon. Since the amorphous silicon layer is fixed at the substrate, this will lead to large stress which has to be accommodated by the amorphous structure.

During de-intercalation the reflectivity cannot be fitted by assuming a single Li_xSi layer. A second layer with a smaller SLD

Table 2 Parameters of the best fits for the electrode system for different intercalation steps. The fit parameters of the quartz block, of the palladium layer, of the electrolyte and of the intermediate layer as given in Table 1 for the virgin state are kept fixed during the fit. The + indicates an additional (de-)intercalation step. For details see the text

		Amorphous silicon			Surface layer per SEI		
		Thickness (Å)	SLD ($\times 10^{-6}$ Å^{-2})	Roughness (Å)	Thickness (Å)	SLD ($\times 10^{-6}$ Å^{-2})	Roughness (Å)
Intercalation step							
0	Virgin	425 ± 25	1.95 ± 0.05	14 ± 3	—	—	—
1	20 μA for 1 h	425 ± 25	1.95 ± 0.05	14 ± 3	—	—	—
2	+100 μA for 1 h	544 ± 17	1.67 ± 0.08	4 ± 4	—	—	—
3	+100 μA for 2 h	769 ± 10	1.00 ± 0.17	10 ± 5	—	—	—
De-intercalation step							
4	+100 μA for 1 h	424 ± 9	1.68 ± 0.12	5 ± 5	74 ± 8	1.33 ± 0.13	0
5	+100 μA for 9 min	414 ± 14	1.61 ± 0.18	20 ± 6	20 ± 5	0.71 ± 0.23	0

Table 3 Intercalation–de-intercalation time, overall specific capacity, overall relative Li fraction, x, and calculated SLD as expected for the different intercalation steps. The data are calculated according to eqn (1)–(3)

	Intercalation time (s)	Theoretical specific capacity (eqn (1)) (A h g^{-1})	Relative Li fraction x (eqn (2)) (Li$_x$Si)	Calculated SLD$_{theo}$ (eqn (3)) ($\times 10^{-6}$ Å^{-2})
Intercalation step				
2	3600	0.83	0.87	0.73
3	7200	2.50	2.61	−0.14
De-intercalation step				
4	3600	1.67	1.75	0.18
5	530	1.54	1.62	0.24

and a higher Li concentration has to be introduced for appropriate fitting (see Table 2). The neighbouring interface roughnesses were set to zero for an adequate description. This second layer can be tentatively attributed to the SEI. Consequently, the present study indicates that a measurable SEI (by NR) is mainly formed during de-intercalation. This interesting and surprising effect is probably correlated with recent *ex situ* observations[9] where strong modification of the SEI during an intercalation cycle is detected and should be investigated in more detail in future.

In the literature, it is stated that each incorporated Li atom will expand the Si lattice by $\Delta V = 14.7$ Å^3,[39] where the volume of a Si atom is $V_{Si} = 21.3$ Å^3. Now, the SLD of Li$_x$Si is given theoretically by

$$\mathrm{SLD}_{\mathrm{theo}} = \frac{b_{\mathrm{Si}} + x b_{\mathrm{Li}}}{V_{\mathrm{Li}_x\mathrm{Si}}} \qquad (3)$$

where $b_{Si} = 4.15$ fm and $b_{Li} = -1.90$ fm are the bound coherent neutron lengths of Si and Li, respectively, and $V_{\mathrm{Li}_x\,\mathrm{Si}} = \Delta V x + V_{Si}$ is the molecular volume of a Li$_x$Si unit. The SLDs calculated from eqn (3) are also given in Table 3 together with the corresponding values of specific capacity and Li content as determined from eqn (1) and (2).

In Fig. 6 the difference, ΔSLD, between the SLDs of the Li$_x$Si layer as obtained from the experiments and the corresponding fits (SLD$_{exp}$) (see Table 2) and of the theoretically calculated values from eqn (2) and (3) (SLD$_{theo}$) (see Table 3) is plotted against time. Obviously, the experimental values are all higher than the theoretically expected values. This means actually that the NR experiments detect a lower Li content in the silicon layer

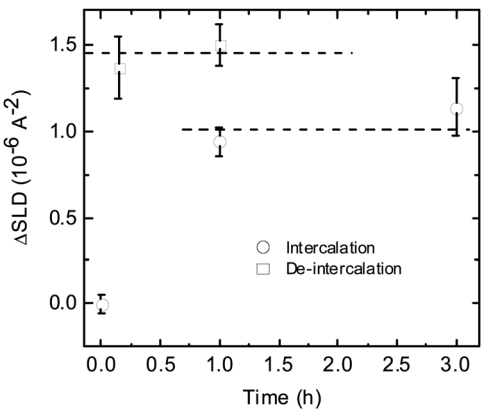

Fig. 6 Difference, ΔSLD = SLD$_{exp}$ − SLD$_{theo}$, of experimentally determined SLD$_{exp}$ of the Li$_x$Si layer (Parratt32 fitting) and calculated SLD$_{theo}$ of that layer (eqn (3)) as a function of intercalation–de-intercalation time.

than expected from the applied intercalation time. The reason for this finding is unclear at the moment. A possible explanation might be that, during intercalation, in addition to lithium, which lowers the SLD, small amounts of Cl and O from the electrolyte also penetrate the silicon layer which will enhance the SLD. Chlorine has a very high scattering length of 9.577 fm compared to that of silicon (4.15 fm) and of lithium (−1.90 fm). Consequently only small portions of Cl will enhance the SLD significantly. For future studies the amount of Cl and O inside the electrode will be examined (*e.g. ex situ* by X-ray Photo Electron Spectroscopy). Of interest might be also the use of isotope labelled $^6LiClO_4$ in order to identify exactly the amount

of Li incorporated into the electrode. As further obvious from Fig. 6, the SLDs of the amorphous Li_xSi layer corresponding to the de-intercalation process are lower than those in the intercalation process. This is attributed to the fact that during de-lithiation a detectable SEI is formed where additional Li is expected to be stored.

4. Conclusion

We constructed and tested a closed three-electrode electrochemical cell for the *in operando* investigation of the intercalation of lithium into amorphous silicon electrodes in lithium-ion batteries by neutron reflectometry. The following important results were achieved: (i) the penetration of lithium into amorphous silicon can effectively be monitored during charging and discharging by changes in the scattering length density. The results indicate a constant Li concentration inside the electrode. (ii) The measurements allow us to detect the volume expansion/reduction of amorphous silicon during lithiation/de-lithiation caused by the modification of the silicon host by lithium. (iii) During de-lithiation the formation of a several nanometer thin lithium rich surface layer can be observed, which might be identified with the solid electrolyte interface (SEI). (iv) Finally, irreversible charge losses after complete de-intercalation were found in the experiments, which are caused by the existence of the lithium rich surface layer and small amounts of residual lithium in the silicon electrode.

The experimental design of the cell is the base for future *in situ* studies on intercalation processes at the electrolyte/electrode interfaces as well as quantification of intercalation kinetics and of intercalation pathways. The unexpected result on the formation of the SEI during de-intercalation will be investigated in more detail during further NR experiments in combination with *ex situ* X-ray Photoelectron Spectroscopy and high resolution Secondary Ion Mass Spectrometry.

Acknowledgements

Financial support from the Deutsche Forschungsgemeinschaft (DFG) in the framework of the focus program SPP 1473 ('WenDeLIB') is gratefully acknowledged. We thank R. Deichmann for the design of Fig. 1, K. Stallberg for performing the AFM measurements, I. Hanzu (U Hannover) for fruitful discussions and the Helmholtz-Zentrum Berlin für Materialien und Energie for providing beamtime.

References

1 *High Energy Density Lithium Batteries*, *Materials, Engineering, Applications*, ed. K. E. Aifantis, S. A. Hackney and R. V. Kumar, Wiley–VCH, 2010.
2 *Lithium-Ion Batteries: Science and Technologies*, ed. M. Yoshio, R. J. Brodd and A. Kozawa, Springer, 2010.
3 *Lithium-Ion Batteries: Advanced Materials and Technologies*, ed. X. Yuan, H. Liu and J. Zhang, CRC Press Inc, 2011.
4 F. T. Wagner, B. Lakshmanan and M. F. Mathias, *J. Phys. Chem. Lett.*, 2010, **1**, 2204.
5 P. G. Bruce, B. Scrosati and J.-M. Tarascon, *Angew. Chem., Int. Ed.*, 2008, **47**, 2930–2946.
6 S. C. Nagpurea, R. G. Downing, B. Bhushana, S. S. Babuc and L. Caod, *Electrochim. Acta*, 2011, **56**, 4735.
7 Z. Remes, M. Vanecek, P. Torres, U. Kroll, A. H. Mahan and R. S. Crandall, *J. Non-Cryst. Solids*, 1998, **227–230**, 876.
8 D. E. Arreaga-Salas, A. K. Sra, K. Roodenko, Y. J. Chabal and C. L. Hinkle, *J. Phys. Chem. C*, 2012, **116**, 9072.
9 C. C. Nguyen, S.-W. Woo and S.-W. Song, *J. Phys. Chem. C*, 2012, **116**, 14764.
10 S. Murugesan, J. T. Harris, B. A. Korgel and K. J. Stevenson, *Chem. Mater.*, 2012, **24**, 1306.
11 B. Philippe, R. Dedryvère, J. Allouche, F. Lindgren, M. Gorgoi, H. Rensmo, D. Gonbeau and K. Edström, *Chem. Mater.*, 2012, **24**, 1107.
12 S. F. Amalraj and D. Aurbach, *J. Solid State Electrochem.*, 2011, **15**, 877.
13 C. M. Wang, X. Li, Z. Wang, W. Xu, J. Liu, F. Gao, L. Kovarik, J.-G. Zhang, J. Howe, D. J. Burton, Z. Liu, X. Xiao, S. Thevuthasan and D. R. Baer, *Nano Lett.*, 2012, **12**, 51624.
14 D. Ruzmetov, V. P. Oleshko, P. M. Haney, H. J. Lezec, K. Karki, K. H. Baloch, A. K. Agrawal, A. V. Davydov, S. Krylyuk, Y. Liu, J. Y. Huang, M. Tanase, J. Cumings and A. A. Talin, *Nano Lett.*, 2012, **12**, 505.
15 N. Balke, S. Jesse, Y. Kim, L. Adamczyk, A. Tselev, I. N. Ivanov, N. J. Dudney and S. V. Kalinin, *Nano Lett.*, 2010, **10**, 3420.
16 M. Klett, M. Giesecke, A. Nyman, F. Hallberg, R. W. Lindström, G. Lindbergh and I. Furo, *J. Am. Chem. Soc.*, 2012, **134**, 14654.
17 L. Y. Beaulieu, T. D. Hatchard, A. Bonakdarpour, M. D. Fleischauer and J. R. Dahn, *J. Electrochem. Soc.*, 2003, **150**, A1457.
18 J. Li and J. R. Dahn, *J. Electrochem. Soc.*, 2007, **154**, A156.
19 M. Morcrette, Y. Chabre, G. Vaughan, G. Amatucci, J.-B. Leriche, S. Patoux, C. Masquelier and J.-M. Tarascon, *Electrochim. Acta*, 2002, **47**, 3137.
20 P. M. Saville, M. Gonsalves, A. R. Hillman and R. Cubitt, *J. Phys. Chem. B*, 1997, **101**, 1.
21 A. Glidle, A. R. Hillman, K. S. Ryder, E. L. Smith, J. Cooper, N. Gadegaard, J. R. P. Webster, R. Dalgliesh and R. Cubitt, *Langmuir*, 2009, **25**, 4093.
22 A. Glidle, P. E. Pearson, E. L. Smith, J. M. Cooper, R. Cubitt, R. M. Dalgliesh, A. R. Hillman and K. S. Ryder, *J. Phys. Chem. B*, 2007, **111**, 4043.
23 I. Zawisza, I. Burgess, G. Szymanski, J. Lipkowski, J. Majewski and S. Satija, *Electrochim. Acta*, 2004, **49**, 3651.
24 M. Schönhoff, V. Ball, A. R. Bausch, C. Dejugnat, N. Delorme, K. Glinel, R. v. Klitzing and R. Steitz, *Colloids Surf., A*, 2007, **303**, 14.
25 S. Singh, S. Basu and S. K. Ghosh, *Appl. Surf. Sci.*, 2009, **255**, 5910.
26 S. Singh, S. Basu, A. K. Poswal, R. B. Tokas and S. K. Ghosh, *Corros. Sci.*, 2009, **51**, 575.

27 M. Wagemaker, R. van de Krol and A. A. van Well, *Physica B*, 2003, **336**, 124–129.
28 J. E. Owejan, J. P. Owejan, S. C. DeCaluwe and J. A. Dura, *Chem. Mater.*, 2012, **24**, 2133.
29 X.-L. Wang, K. An, L. Cai, Z. Feng, S. E. Nagler, C. Daniel, K. J. Rhodes, A. D. Stoica, H. D. Skorpenske, C. Liang, W. Zhang, J. Kim, Y. Qi and S. J. Harris, *Sci. Rep.*, 2012, **2**, 747.
30 C. A. Bridges, X.-G. Sun, J. Zhao, M. P. Paranthaman and S. Dai, *J. Phys. Chem. C*, 2012, **116**, 7701.
31 J. F. M. Oudenhoven, F. Labohm, M. Mulder, R. A. H. Niessen, F. M. Mulder and P. H. L. Notten, *Adv. Mater.*, 2011, **23**, 4103.
32 D. Goers, M. Holzapfel, W. Schweifele, E. Lehmann, P. Vontobel and P. Novak, *J. Power Sources*, 2004, **130**, 221.
33 S. Bourderau, T. Brousse and D. M. Schleich, *J. Power Sources*, 1999, **81–82**, 233–236.
34 H. Jung, M. Park, S. H. Han, H. Lim and S.-K. Joo, *Solid State Commun.*, 2003, **125**, 387.
35 S. Ohara, J. Suzuki, K. Sekine and T. Takamura, *J. Power Sources*, 2004, **136**, 303.
36 V. Baranchugov, E. Markevich, E. Pollak, G. Salitra and D. Aurbach, *Electrochem. Commun.*, 2007, **9**, 796.
37 L. F. Nazar and O. Crosnier, in *Lithium Batteries*, ed. G.-A. Nazri and G. Pistoia, Springer, 2009, p. 129.
38 T. Takamura, S. Ohara, M. Uehara, J. Suzuki and K. Sekine, *J. Power Sources*, 2004, **129**, 96.
39 V. L. Chevrier and J. R. Dahn, *J. Electrochem. Soc.*, 2009, **156**, A454.
40 T. D. Hatchard and J. R. Dahn, *J. Electrochem. Soc.*, 2004, **151**, A838.
41 Y. Kubota, M. C. S. Escaño, H. Nakanishi and H. Kasai, *J. Appl. Phys.*, 2007, **102**, 053704.
42 C. Braun, *Parratt32 or The Reflectivity Tool, Version 1.6.0*, 1997–2002.
43 H. Lutz, M. Bruns, F. Link and H. Baumann, *Thin Solid Films*, 1998, **332**, 230.
44 http://www.ncnr.nist.gov/resources/sldcalc.html.
45 K. W. Schroder, H. Celio, L. J. Webb and K. J. Stevenson, *J. Phys. Chem. C*, 2012, **116**, 19737.
46 T. L. Kulova and A. M. Skundin, *Russ. J. Electrochem.*, 2012, **48**, 330.
47 T. L. Kulova, *Russ. J. Electrochem.*, 2008, **44**, 569.
48 A. M. James and M. P. Lord, *Macmillan's Chemical and Physical Data*, Macmillan, London, UK, 1992.
49 In *CRC Handbook of Chemistry and Physics*, ed. W. M. Haynes, CRC Press, 92nd edn, 2012.
50 N. N. Greenwood and A. Earnshaw, *Chemistry of the Elements*, Pergamon Press, Oxford, 1984, p. 393.
51 F. Dalard, M. Ulmann, J. Augustynski and P. Selvam, *J. Electroanal. Chem.*, 1989, **270**, 445.

